Fundamental Limits to Extinction by Metallic Nanoparticles

O. D. Miller,[1,*] C. W. Hsu,[2,3] M. T. H. Reid,[1] W. Qiu,[2] B. G. DeLacy,[4] J. D. Joannopoulos,[2] M. Soljačić,[2] and S. G. Johnson[1]
[1]Department of Mathematics, Massachusetts Institute of Technology, Cambridge, Massachusetts 02139, USA
[2]Department of Physics, Massachusetts Institute of Technology, Cambridge, Massachusetts 02139, USA
[3]Department of Physics, Harvard University, Cambridge, Massachusetts 02138, USA
[4]U.S. Army Edgewood Chemical Biological Center, Research and Technology Directorate, Aberdeen Proving Ground, Maryland 21010, USA
(Received 6 November 2013; published 26 March 2014)

We show that there are shape-independent upper bounds to the extinction cross section per unit volume of dilute, randomly arranged nanoparticles, given only material permittivity. Underlying the limits are restrictive sum rules that constrain the distribution of quasistatic eigenvalues. Surprisingly, optimally designed spheroids, with only a single quasistatic degree of freedom, reach the upper bounds for four permittivity values. Away from these permittivities, we demonstrate computationally optimized structures that surpass spheroids and approach the fundamental limits.

DOI: 10.1103/PhysRevLett.112.123903 PACS numbers: 42.25.Bs, 02.70.-c, 41.20.-q, 78.20.Bh

Many applications [1–8] employ disordered collections of particles to absorb or scatter light, and the extinction for a given total particle volume (for a dilute system in which coagulation and multiple scattering are negligible) is determined by the total extinction (scattering + absorption) cross section per unit volume σ_{ext}/V of the individual particles [9,10]. In this Letter, we prove fundamental upper bounds on σ_{ext}/V for small metallic particles of any shape, we show that previous work on maximizing particle scattering [10–14] (including "superscattering" [15–17]) was a factor of 6 or more from these bounds, and we employ a combination of analytical results and large-scale optimization ("inverse" design) to discover nearly optimal particle shapes. Most previous work in this area was confined to spheres [10,12,16,18,19] or a few high-symmetry shapes [11,13–15,17], whereas we optimize numerically over shapes with ≈1000 free parameters (and prove our theorem for completely arbitrary shapes) over the visible spectrum, and we also consider coated multimaterial shapes. We find that the optimal σ_{ext}/V is invariably obtained for subwavelength particles where absorption dominates and the quasistatic approximation applies. We can then apply a little-known eigenproblem formulation of quasistatic electromagnetism in terms of "resonances" in the permittivity ϵ (*not* in the frequency ω) [20–24], and we employ various sum rules of these resonances [20,25,26] to derive a bound on the cross section. Surprisingly, very different optimized shapes (such as ellipsoids or "pinched" tetrahedra) exhibit nearly identical $\sigma_{\text{ext}}(\omega)$ spectra (greatly superior to nonoptimized particles) once σ_{ext} is averaged over incident angle, a result we can explain in terms of the quasistatic resonances. Finally, we explain how our bounds provide materials guidance in various wavelength regimes, with potential applications ranging from cancer therapy [1–3] and plasmonic biosensors [4–6,27] to next-generation solar cells [28] and optical couplers [29].

Some previous bounds on optical properties of dilute particle suspensions have been derived [30–34]. Purcell derived a sum rule limiting the integral over all frequencies of extinction by spheroids [35]. The limit has been extended to a variety of materials and structures [30–33], but is geometry dependent and difficult to apply as a general rule. Alternatively, many authors have bounded the effective "metamaterial" permittivity of composite media [36–39], a related but not identical problem. The methods presented here, applied to the effective permittivity of a lossless dielectric, are able to reproduce the well-known Hashin-Strikman bounds [40,41] of composite theory.

A single numerical optimization conceptually demonstrates many key findings for nanoparticle extinction. To illustrate, we design a silver particle, for maximum frequency- and angle-averaged extinction cross section per unit volume, σ_{ext}/V, over a 33 nm bandwidth at center wavelength $\lambda = 437$ nm ($Q = 13$). We do not impose quasistatic conditions *a priori*; we employ the full Maxwell equations. Ultimately, the optimizations always converged to very small, essentially quasistatic sizes, and there is reason to believe that such quasistatic sizes may be globally optimal for metals. For quasistatic particles (size approaches 0), σ/V is a constant. As the particle size increases and moves away from the quasistatic limit, the number of surface modes increases proportional to the surface area, so σ/V decreases. Further size increases reach the geometric-optics limit, where $\sigma/V \to 0$ as $V \to \infty$.

We employed a number of techniques to make the optimization tractable. To quickly solve Maxwell's equations, we used a free-software implementation [42,43] of the boundary-element method [44]. Angle averaging is essentially free with such a solver. In many applications, the figure

Report Documentation Page

Form Approved
OMB No. 0704-0188

1. REPORT DATE	2. REPORT TYPE	3. DATES COVERED
26 MAR 2014		**00-00-2014 to 00-00-2014**

4. TITLE AND SUBTITLE	5a. CONTRACT NUMBER
Fundamental Limits to Extinction by Metallic Nanoparticles	5b. GRANT NUMBER
	5c. PROGRAM ELEMENT NUMBER
6. AUTHOR(S)	5d. PROJECT NUMBER
	5e. TASK NUMBER
	5f. WORK UNIT NUMBER
7. PERFORMING ORGANIZATION NAME(S) AND ADDRESS(ES) **Massachusetts Institute of Technology,Department of Mathematics,77 Massachusetts Avenue,Cambridge,MA,02139**	8. PERFORMING ORGANIZATION REPORT NUMBER
9. SPONSORING/MONITORING AGENCY NAME(S) AND ADDRESS(ES)	10. SPONSOR/MONITOR'S ACRONYM(S)
	11. SPONSOR/MONITOR'S REPORT NUMBER(S)

12. DISTRIBUTION/AVAILABILITY STATEMENT
Approved for public release; distribution unlimited

13. SUPPLEMENTARY NOTES

14. ABSTRACT

15. SUBJECT TERMS

16. SECURITY CLASSIFICATION OF:			17. LIMITATION OF ABSTRACT	18. NUMBER OF PAGES	19a. NAME OF RESPONSIBLE PERSON
a. REPORT	b. ABSTRACT	c. THIS PAGE			
unclassified	**unclassified**	**unclassified**	**Same as Report (SAR)**	**5**	

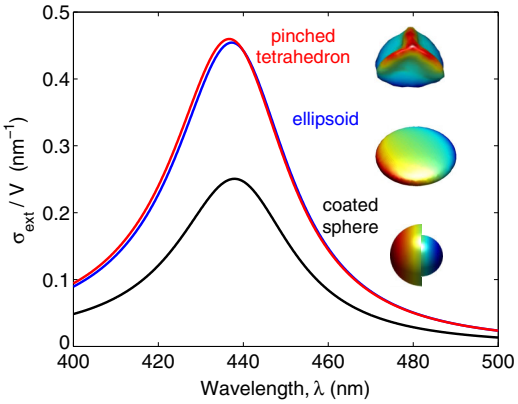

FIG. 1 (color online). Angle-averaged extinction cross section per unit volume of computationally optimized Ag particles, designed for $\lambda_0 = 437$ nm and $\Delta\lambda = 33$ nm. An ellipsoid provides almost twice the extinction of an optimally coated sphere, but optimizing over ≈1000 spherical harmonics basis functions yields only a 2% further improvement, due to fundamental limits on the eigenvalue distribution. Surface coloring depicts the charge density on resonance, where $\epsilon_{\mathrm{Ag}}(437\ \mathrm{nm}) \approx -5.5 + 0.7i$. Particle dimensions are ≈10 nm.

of merit is a frequency-averaged extinction, defined by the integral $\sigma_{\mathrm{ext}} = \int \sigma_{\mathrm{ext}}(\omega) H_{\Delta\omega}(\omega) d\omega$. We efficiently compute this integral by contour integration, which for a Lorentzian H of bandwidth $\Delta\omega$ reduces to a *single* scattering problem at a *complex* frequency $\omega_0 + i\Delta\omega$ [45–47]. For optimization, the particle shape was parametrized by the zero level set of a sum of spherical harmonics [48], i.e., $r(\theta,\phi) = \sum_{lm} c_{lm} Y_{lm}(\theta,\phi)$ (restricting us to "star-shaped" structures). Given the gradient of the objective with respect to these ≈1000 degrees of freedom (efficiently computed by an adjoint method [49–51]), we employ a free-software implementation [52] of standard nonlinear optimization algorithms [53] to find a local optimum from a given starting point. We also optimized the few degrees of freedom of coated spheres and ellipsoids for the sake of comparison.

Figure 1 depicts the optimal particles and their respective extinction spectra. The optimal designs were in the quasistatic limit, with dimensions ≈10 nm. A 10 nm size is not uniquely optimal, but is rather the size at which performance is dominated by quasistatic response. Doubling the size is clearly worse (≈2%), whereas a tenfold size reduction is better by only 0.2%, within the meshing error. Furthermore, our calculations do not account for the quantum plasmonic properties of very small particles, which would tend to decrease performance below 10 nm dimensions [54].

We see that uncoated ellipsoids provide significant gains over coated spheres, which already provide a substantial response [1,3,10,55] (coated ellipsoids showed no further benefit). This suggests a principle that tuning resonances by geometrical deformation rather than by coatings enhances performance. Oblate ("pancake") ellipsoids are superior to prolate ("rod") ellipsoids, because they couple to two of the three polarizations of randomly oriented incident waves. In the much larger spherical-harmonics design space, the optimal structure turned out to be a "pinched" tetrahedron (PT), which can be conceptualized as pinching a sphere towards the four centroids of the faces of an inscribed tetrahedron. Surprisingly, the much larger design space yielded a structure that was only 2% better than the best ellipsoid. The two structures have very different responses for a given incidence angle and polarization; only when averaged over angle and polarization do the responses become nearly identical. Also shown in Fig. 1 are the imaginary parts of the charge densities for resonant incident waves, explained below. Intuitively, the ellipsoid and PT are better than a coated sphere because the opposing surface charges have larger spatial separations.

The nearly identical spectra for the spheroid and PT can be explained by a fundamental restriction on quasistatic eigenmodes, which are prevented from fully coupling to external radiation. In the quasistatic limit, the incident field is locally constant and the response of the system is determined by induced charge densities at the surfaces. One can construct the fields from the homogeneous Green's functions of the induced surface charges $\sigma(\mathbf{x})$. For a surface S, the surface integral equation for the charge density is [20–24]:

$$\Lambda\sigma(\mathbf{x}) - \underbrace{\int_S \hat{\mathbf{n}}(\mathbf{x})\cdot\mathbf{G}^E(\mathbf{x}-\mathbf{x}')\sigma(\mathbf{x}')dS'}_{\hat{K}\sigma} = \mathbf{E}^{\mathrm{inc}}(\mathbf{x})\cdot\hat{\mathbf{n}}(\mathbf{x}), \quad (1)$$

where $\Lambda = (\epsilon_{\mathrm{int}} + \epsilon_{\mathrm{ext}})/2(\epsilon_{\mathrm{int}} - \epsilon_{\mathrm{ext}})$ relates interior and exterior permittivities, the electrostatic Green's function $\mathbf{G}^E(\mathbf{x}) = \mathbf{x}/4\pi|\mathbf{x}|^3$, and $\mathbf{E}^{\mathrm{inc}}(\mathbf{x})\cdot\hat{\mathbf{n}}(\mathbf{x})$ is the normal component of the incident field at $\mathbf{x}$ (boldface indicates vector quantities). As distinguished from the resonant *frequencies* of Maxwell's equations, there are resonant *permittivities* $\epsilon_{\mathrm{int}}/\epsilon_{\mathrm{ext}}$ for the quasistatic integral equation. These are negative, real-valued permittivities ϵ_n at which self-sustaining charge densities exist without external fields, for specific eigenmodes σ_n satisfying $\hat{K}\sigma_n = \lambda_n\sigma_n$, where $\hat{K}$ is the Neumann-Poincaré integral operator defined by Eq. (1). The eigenvalues λ_n lie in the interval $[-1/2, 1/2]$ [23,24,56], such that $\epsilon_n < 0$. The left eigenvectors of $\hat{K}$, denoted τ_n, have the same eigenvalue spectrum as the σ_n (i.e., $\hat{K}^\dagger\tau_n = \lambda_n\tau_n$) and provide the orthogonality condition $\langle\sigma_n,\tau_m\rangle = \int_S \sigma_n\tau_m dS = \delta_{mn}$ [23].

Equation (1) is valid for linear, isotropic, and nonmagnetic materials. Its generalization to multiple surfaces takes Λ to a diagonal matrix [57]; the eigenmode decomposition of $\hat{K}$ imposes strict requirements on the allowable form of the matrix, such that each interface must separate the same materials. Thus, Eq. (1) is valid for arbitrarily many interacting objects, possibly coated or holey (e.g., torii), as long as there are only two permittivities.

The eigenmodes of $\hat{K}$ contribute to absorption and scattering through α, the particle's polarizability per unit volume V, which relates the incident field to the dipole moment by $p_\ell = V\sum_m \alpha_{\ell m} E^{\mathrm{inc}}_m$. Decomposing the charge density as a superposition of eigenmodes, $\sigma = \sum_n c_n\sigma_n$, solving for c_n via Eq. (1) and for the dipole moment via $\mathbf{p} = \int_S \mathbf{x}\sigma dA$, yields

$$\alpha_{\ell m} = \sum_n \frac{p_n^{\ell m}}{L_n - \xi(\omega)}, \tag{2}$$

where $p_n^{\ell m} = \langle \sigma_n, x_\ell \rangle \langle \tau_n, \hat{n}_m \rangle / V$ is the dipole strength of each mode, $L_n = 1/2 - \lambda_n$ is the depolarization factor, and $\xi(\omega) = -\epsilon_{\text{int}}/(\epsilon_{\text{int}} - \epsilon_{\text{ext}})$ represents the relative properties of the interior and exterior materials.

The distribution of eigenmodes, and therefore the induced susceptibility, is restricted by two crucial sum rules. The first is the f-sum rule [25,58], limiting the total dipole strength for uncoated particles:

$$\sum_n p_n^{\ell m} = \delta_{\ell m}. \tag{3}$$

The total dipole strength of coated particles is reduced by the metallic volume fraction f [58]. The second sum rule [26,58], applicable for coated and uncoated particles, states that the weighted average of the depolarization factors must be $1/3$:

$$\langle L_n \rangle = \frac{\sum_n p_n L_n}{\sum_n p_n} = \frac{1}{3}, \tag{4}$$

where p_n denotes $\sum_\ell p_n^{\ell\ell}$.

A sphere has a depolarization factor of $1/3$, leading to a "plasmon" resonance at $\epsilon \approx -2$ ($\xi = 1/3$). Equation (4) dictates that the average depolarization factor of *every* structure must equal that of the sphere. Although it was exploited for composites with certain symmetries [59,60], this general property has not been widely recognized and is very important in limiting possible extinction rates.

The average extinction of randomly arranged particles is proportional to the imaginary part of $\text{Tr}\alpha_{\ell m}$ [9], which is given by Eq. (2):

$$\frac{\sigma_{\text{ext}}}{V} = \frac{2\pi}{3\lambda} \sum_n \text{Im}\left[\frac{1}{L_n - \xi(\omega)}\right] p_n. \tag{5}$$

A resonance occurs for $L_n = \xi_r(\omega)$, where r and i subscripts denote real and imaginary parts, respectively. For particles in vacuum with susceptibility $\chi(\omega) = \epsilon(\omega) - 1$, $\xi(\omega) = -1/\chi(\omega)$. Only metals, with $\epsilon_r(\omega) < 0$, can achieve $0 < \xi_r < 1$, and therefore exhibit quasistatic surface-plasmon modes. The second sum guarantees that (except in the case $\xi_r = 1/3$) a particle cannot have all of its dipole strength on resonance; there must always be a counterbalancing dipole moment such that $\langle L_n \rangle = 1/3$.

For a given material parameter $\xi_r(\omega)$, we can show that the optimal distribution of eigenmodes has at most two distinct depolarization factors, L_1 and L_2. We have rigorously derived the exact locations of the two eigenvalues [58], but for relevant materials a simple solution suffices:

$$(L_1, L_2) = \begin{cases} (\xi_r, 1) & 0 < \xi_r < 1/3 \\ (0, \xi_r) & 1/3 < \xi_r < 1 \\ (0, 1) & \xi_r < 0 \text{ or } \xi_r > 1, \end{cases} \tag{6}$$

which corresponds to placing as much of the dipole moment as possible on resonance ($L = \xi_r$), and the rest of the dipole strength at the opposite boundary to satisfy the second sum rule. Equation (6) is exact for $\xi_i = 0$ (both a low-loss $\chi_i = 0$ and infinite-loss $\chi_i \to \infty$ limit), but is also very accurate (error $< 10^{-3}$) otherwise. With L_n given by Eq. (6), we can solve for p_n from Eqs. (3) and (4). Plugging L_n and p_n into Eq. (5) yields the upper limit to the extinction per unit volume:

$$\frac{\sigma_{\text{ext}}}{V} \le \frac{2\pi}{3\lambda} \begin{cases} \frac{2\chi_r^3(1+\chi_r)+\chi_i^2(3+2\chi_r+4\chi_r^2)+2\chi_i^4}{\chi_i(\chi_i^2+(1+\chi_r)^2)} & 0 < -\frac{\chi_r}{|\chi|^2} < \frac{1}{3} \\ 3\chi_i - \frac{\chi_r}{\chi_i}|\chi|^2 & \frac{1}{3} < -\frac{\chi_r}{|\chi|^2} < 1 \\ \chi_i\left(2 + \frac{1}{\chi_i^2+(1+\chi_r)^2}\right) & \text{else,} \end{cases} \tag{7}$$

which provides a limit for any possible susceptibility, independent of geometry. Ideal scatterers are uncoated, and have metallic permittivities with small imaginary parts (as in Ref. [19]) and very negative real parts; for $\epsilon_i \ll |\epsilon_r|$, Eq. (7) simplifies to

$$\frac{\sigma_{\text{ext}}}{V} \le \frac{4\pi}{3\lambda} \frac{\epsilon_r^2}{\epsilon_i} + O(\epsilon_i), \tag{8}$$

where the "O" notation indicates the asymptotic scaling of the higher-order term.

Equations (7) and (8) represent fundamental limits to quasistatic particle extinction. Figure 2 illustrates these limits by normalizing them relative to the value of extinction on resonance, $\sigma_{\text{res}} = 2\pi/3\lambda\xi_i(\omega)$, and comparing them to ellipsoid limits computed through nonlinear optimization [52]. The structural eigenmodes were computed with boundary-element method software [61]. $\sigma_{\text{ext}}/\sigma_{\text{res}}$ can be thought of as the number of fully coupled polarizations; only at $\xi_r = 1/3$ ($\epsilon_r \approx -2$) can full coupling to all three polarizations occur. Thus we see why ellipsoids perform very well, and why the optimal structure of Fig. 1 barely outperformed the ideal ellipsoid: in many cases, full coupling to two polarizations closely approaches the ideal performance. This is exactly true for $\epsilon_r \to -\infty$, one of the cases in which ellipsoids reach the upper bound. The other three cases are $\epsilon_r = -2$, $\epsilon_r = -1$, and $\epsilon_r = 0$, for which a sphere, infinite cylinder, and infinitely thin disk are optimal, respectively. In each case, the spheroid depolarization factors [9] are identical to those of the optimal general shape, given by Eq. (6).

Included in Fig. 2 are optimizations at other permittivities (assuming the complex permittivity of Ag); there is a family of "pinched tetrahedron" structures that emerge as superior design choices over ellipsoids. It is important to note that spheres are not globally optimal, as the normalization factor σ_{res} is a function of ϵ_r. The inset shows the absolute extinction, which scales as ϵ_r^2/ϵ_i.

The limits of Eqs. (7) and (8) may appear to contradict arguments in coupled-mode theory (CMT) [16,62], but in fact do not. CMT predicts $\sigma_{\text{ext}} \sim \lambda^2$ scaling only when radiation loss dominates over absorption loss; when

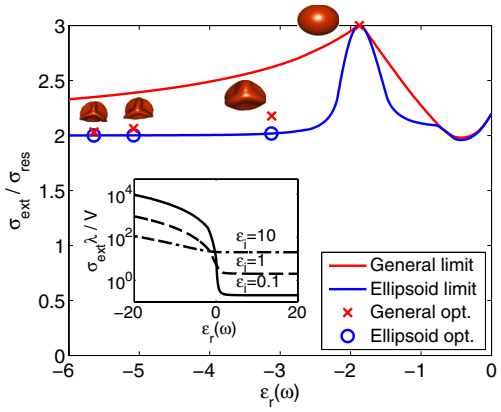

FIG. 2 (color online). Fundamental extinction limits, given by Eq. (7) and normalized to the maximum extinction of a single-polarization resonance σ_{res}. Spheres are not optimal for absolute σ_{ext} (see inset), but do enable full coupling to three polarizations, given by the normalized value $\sigma_{\text{ext}}/\sigma_{\text{res}}$. Markers indicate computationally optimized structures. $\epsilon_i(\omega)$ is taken to be that of Ag, although this has only a small effect on the line shape. Ellipsoids can approach the general bounds in four limits: $\epsilon_r \to -\infty$ (oblate disk), $\epsilon_r = -2$ (sphere), $\epsilon_r = -1$ (cylinder), and $\epsilon_r = 0$ (oblate disk). Computationally optimized pinched tetrahedra improve upon ellipsoids at intermediate $\epsilon_r(\omega)$. Inset: upper bound on $\sigma_{\text{ext}}\lambda/V$, which increases with ϵ_r^2/ϵ_i ($\epsilon_r < 0$).

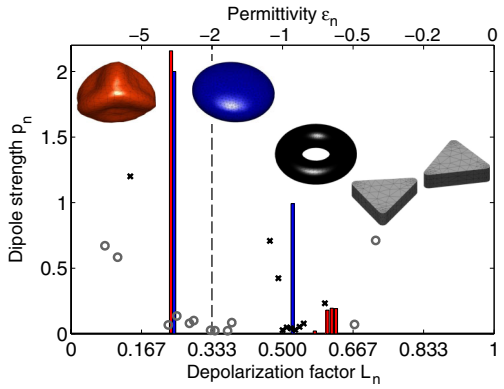

FIG. 3 (color online). Distributions of dipole strength for computationally optimal [pinched tetrahedron (PT)], nearly optimal (ellipsoid), and nonoptimal (torus and bow-tie antenna) structures subject to the bounds of Eq. (7). The PT and ellipsoid have degenerate modes at the optimization permittivity, in this case $\epsilon_r(\omega) = -3.2$. The PT outperforms the ellipsoid because its "undesirable" eigenmodes are closer to $L = 1$, enabling a larger dipole strength at $L_1 = 0.24$ ($\epsilon_1 = -3.2$). Equally important is the lack of other bright modes; e.g., torii (crosses) and bow-tie antennas (open circles) have disperse modes, reducing overall extinction. The PT/ellipsoid modes coincide at $L_1 = 0.24$ but are split for visualization.

absorption dominates, CMT predicts $\sigma_{\text{ext}} \sim V/\lambda$, as in Eqs. (7) and (8). Absorption loss dominates for $(2\pi a/\lambda)^3 \ll \epsilon_i$ (Refs. [18,63]), which is satisfied by all quasistatic metallic particles in the visible and infrared.

Figure 3 shows the depolarization factor distributions of the ideal pinched tetrahedron and ellipsoid structures, as well as nonideal structures. We see that the dipole moments are largely concentrated at the desired permittivity, except as required to keep the centroid of L_n equal to $1/3$. The tetrahedra have the off-resonance dipole moments distributed closer to the boundary $L_n = 1$ than ellipsoids, explaining the slightly superior performance.

Figure 4 illustrates the general utility of the bounds of Eq. (7). For a given permittivity, a maximum extinction per unit volume can be computed independent of structure. This has important implications for material selection, which varies by application and frequency. Although the bounds are quasistatic, as discussed earlier the quasistatic bound may be globally optimal. Indeed, the infrared extinction limits are 3 orders of magnitude larger than the best nonquasistatic particles investigated to date [7]. Although the bounds are for a single frequency, through complex-frequency calculations, or known material quality factors (geometry-independent [64]), rational design for any bandwidth is possible.

We can compare our structures to recently proposed "superscattering" structures [15–17]. Of primary importance is the figure of merit (FOM). For applications, volume or weight is the relevant normalization. Normalizing by λ^2, as in [15–17], favors larger particles approaching wavelength scale. A smaller particle with larger σ_{ext}/V likely cannot extinguish a full square wavelength. Yet a dilute mixture of such particles could, with much smaller volumes. As an example, *two* quasistatic nanoellipsoids, with an 8:1 major to minor axis ratio can achieve the same $\sigma_{\text{ext}}/\lambda^2$ as the single particle in [16], while requiring $1/270$th of the volume. A single "channel" in a nonspherical structure can extinguish much more strongly than multiple channels in a spherical structure.

Small, absorbing nanoparticles show promise for a variety of scientific and technical applications. Experimentally approaching the limits derived here would already represent a significant achievement. A possible further improvement could come from harnessing exotic material systems [55,66],

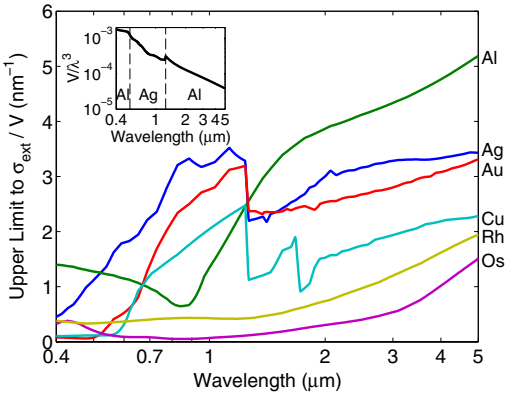

FIG. 4 (color online). Shape-independent fundamental limit to extinction per unit volume for the highest-performing metals [65] at visible and infrared wavelengths. A mixture of Al and Ag nanoparticles, properly designed, could provide ideal extinction over the visible and near- to midinfrared. Inset: minimum volume fraction V/λ^3 required for $\sigma_{\text{ext}} = \lambda^2$. It is possible to achieve λ^2 cross sections for $V/\lambda^3 < 10^{-3}$.

where geometry-dependent material resonances cannot be modeled with bulk permittivities.

This work was supported by the Army Research Office through the Institute for Soldier Nanotechnologies under Contract No. W911NF-07-D0004, and by the AFOSR Multidisciplinary Research Program of the University Research Initiative (MURI) for Complex and Robust On-chip Nanophotonics under Grant No. FA9550-09-1-0704.

*Corresponding author.
odmiller@math.mit.edu

[1] C. Loo, A. Lowery, N. Halas, J. West, and R. Drezek, Nano Lett. **5**, 709 (2005).
[2] D. Peer, J. M. Karp, S. Hong, O. C. Farokhzad, R. Margalit, and R. Langer, Nat. Nanotechnol. **2**, 751 (2007).
[3] E. Boisselier and D. Astruc, Chem. Soc. Rev. **38**, 1759 (2009).
[4] J. N. Anker, W. P. Hall, O. Lyandres, N. C. Shah, J. Zhao, and R. P. Van Duyne, Nat. Mater. **7**, 442 (2008).
[5] W.-S. Chang, J. W. Ha, L. S. Slaughter, and S. Link, Proc. Natl. Acad. Sci. U.S.A. **107**, 2781 (2010).
[6] M. Ohmachi, Y. Komori, A. H. Iwane, F. Fujii, T. Jin, and T. Yanagida, Proc. Natl. Acad. Sci. U.S.A. **109**, 5294 (2012).
[7] P. G. Appleyard, J. Opt. A **9**, 278 (2007).
[8] W.-S. Chang, B. A. Willingham, L. S. Slaughter, B. P. Khanal, L. Vigderman, E. R. Zubarev, and S. Link, Proc. Natl. Acad. Sci. U.S.A. **108**, 19879 (2011).
[9] C. F. Bohren and D. R. Huffman, *Absorption and Scattering of Light by Small Particles* (John Wiley & Sons, New York, 1983).
[10] W. Qiu, B. G. Delacy, S. G. Johnson, J. D. Joannopoulos, and M. Soljačić, Opt. Express **20**, 18494 (2012).
[11] S. Link, M. B. Mohamed, and M. A. El-Sayed, J. Phys. Chem. B **103**, 3073 (1999).
[12] P. K. Jain, K. S. Lee, I. H. El-Sayed, and M. A. El-Sayed, J. Phys. Chem. B **110**, 7238 (2006).
[13] J. Zhu, J.-j. Li, and J.-w. Zhao, Appl. Phys. Lett. **99**, 101901 (2011).
[14] C. E. Román-Velázquez and C. Noguez, J. Chem. Phys. **134**, 044116 (2011).
[15] Z. Ruan and S. Fan, Phys. Rev. Lett. **105**, 013901 (2010).
[16] Z. Ruan and S. Fan, Appl. Phys. Lett. **98**, 043101 (2011).
[17] L. Verslegers, Z. Yu, Z. Ruan, P. B. Catrysse, and S. Fan, Phys. Rev. Lett. **108**, 083902 (2012).
[18] M. I. Tribelsky, Europhys. Lett. **94**, 14004 (2011).
[19] B. S. Luk'yanchuk, A. E. Miroshnichenko, M. I. Tribelsky, Y. S. Kivshar, and A. R. Khokhlov, New J. Phys. **14**, 093022 (2012).
[20] R. Fuchs, Phys. Rev. B **11**, 1732 (1975).
[21] F. Ouyang and M. Isaacson, Philos. Mag. B **60**, 481 (1989).
[22] F. J. García de Abajo and A. Howie, Phys. Rev. B **65**, 115418 (2002).
[23] I. D. Mayergoyz, D. R. Fredkin, and Z. Zhang, Phys. Rev. B **72**, 155412 (2005).
[24] O. D. Kellogg, *Foundations of Potential Theory* (Dover Publications, Inc., New York, 1929).
[25] S. P. Apell, P. M. Echenique, and R. H. Ritchie, Ultramicroscopy **65**, 53 (1996).
[26] R. Fuchs and S. H. Liu, Phys. Rev. B **14**, 5521 (1976).
[27] S. Lal, S. Link, and N. J. Halas, Nat. Photonics **1**, 641 (2007).
[28] H. A. Atwater and A. Polman, Nat. Mater. **9**, 205 (2010).
[29] J. Lin, J. P. B. Mueller, Q. Wang, G. Yuan, N. Antoniou, X.-C. Yuan, and F. Capasso, Science **340**, 331 (2013).
[30] M. Gustafsson, C. Sohl, and G. Kristensson, Proc. R. Soc. A **463**, 2589 (2007).
[31] C. Sohl, M. Gustafsson, and G. Kristensson, J. Phys. A **40**, 11165 (2007).
[32] C. Sohl, M. Gustafsson, and G. Kristensson, J. Phys. D **40**, 7146 (2007).
[33] C. Sohl, M. Gustafsson, and G. Kristensson, J. Acoust. Soc. Am. **122**, 3206 (2007).
[34] A. B. Kostinski and A. Mongkolsittisilp, J. Quant. Spectrosc. Radiat. Transfer **131**, 194 (2013).
[35] E. M. Purcell, Astrophys. J. **158**, 433 (1969).
[36] D. J. Bergman, Phys. Rev. B **19**, 2359 (1979).
[37] D. J. Bergman, Phys. Rev. B **23**, 3058 (1981).
[38] G. W. Milton, J. Appl. Phys. **52**, 5286 (1981).
[39] G. W. Milton, *The Theory of Composites* (Cambridge University Press, Cambridge, England, 2002).
[40] Z. Hashin and S. Shtrikman, J. Mech. Phys. Solids **11**, 127 (1963).
[41] R. Lipton, J. Mech. Phys. Solids **41**, 809 (1993).
[42] M. T. H. Reid and S. G. Johnson, arXiv:1307.2966.
[43] M. T. H. Reid, http://homerreid.com/scuff-EM.
[44] R. F. Harrington, *Field Computation by Moment Methods* (IEEE Press, Piscataway, NJ, 1993).
[45] H. Hashemi, C.-W. Qiu, A. P. McCauley, J. D. Joannopoulos, and S. G. Johnson, Phys. Rev. A **86**, 013804 (2012).
[46] X. Liang, Ph. D. thesis, Massachusetts Institute of Technology, 2013.
[47] X. Liang and S. G. Johnson, Opt. Express **21**, 30812 (2013).
[48] E. J. Garboczi, Cement and Concrete Research **32**, 1621 (2002).
[49] G. Strang, *Computational Science and Engineering* (Wellesley-Cambridge Press, Wellesley, MA, 2007).
[50] J. Jensen and O. Sigmund, Laser Photonics Rev. **5**, 308 (2011).
[51] O. D. Miller, Ph. D. thesis, University of California, Berkeley, 2012.
[52] S. G. Johnson, http://ab-initio.mit.edu/nlopt.
[53] K. Svanberg, SIAM J. Optim. **12**, 555 (2002).
[54] J. A. Scholl, A. L. Koh, and J. A. Dionne, Nature (London) **483**, 421 (2012).
[55] B. G. Delacy, W. Qiu, M. Soljacic, C. W. Hsu, O. D. Miller, S. G. Johnson, and J. D. Joannopoulos, Opt. Express **21**, 19103 (2013).
[56] T. Sandu, Plasmonics **8**, 391 (2013).
[57] H. Ammari, G. Ciraolo, H. Kang, H. Lee, and G. W. Milton, Arch. Ration. Mech. Anal. **208**, 667 (2013).
[58] See Supplemental Material at http://link.aps.org/supplemental/10.1103/PhysRevLett.112.123903 for details.
[59] D. J. Bergman, Phys. Rep. **43**, 377 (1978).
[60] D. Stroud, Phys. Rev. B **19**, 1783 (1979).
[61] U. Hohenester and A. Trügler, Comput. Phys. Commun. **183**, 370 (2012).
[62] R. E. Hamam, A. Karalis, J. D. Joannopoulos, and M. Soljačić, Phys. Rev. A **75**, 053801 (2007).
[63] M. I. Tribelsky and B. S. Lukyanchuk, Phys. Rev. Lett. **97**, 263902 (2006).
[64] F. Wang and Y. R. Shen, Phys. Rev. Lett. **97**, 206806 (2006).
[65] E. D. Palik, *Handbook of Optical Constants of Solids* (Academic Press, London, 1998).
[66] F. Würthner, T. E. Kaiser, and C. R. Saha-Möller, Angew. Chem., Int. Ed. **50**, 3376 (2011).